International Journal of
Plant Biology

MDPI

Article

Genome-Wide Analysis of the Class III Peroxidase Gene Family in *Physcomitrium patens* and a Search for Clues to Ancient Class III Peroxidase Functions

Vincent P. M. Aparato, Fazle Rabbi, Taylor Madarash, Wyllie A. Brisbourne, Elizabeth I. Barker and Dae-Yeon Suh *

Department of Chemistry and Biochemistry, University of Regina, 3737 Wascana Parkway, Regina, SK S4S 0A2, Canada; vpma2297@gmail.com (V.P.M.A.); frabbi016@gmail.com (F.R.); barker.e@gmail.com (E.I.B.)
* Correspondence: suhdaey@uregina.ca

Abstract: Plant class III peroxidases (PRXs) catalyze generation of reactive oxygen species and oxidation of various compounds including lignin precursors. PRXs function in cell wall metabolism, defense, and stress responses. However, gene redundancy and catalytic versatility have impeded detailed functional characterization of *PRX* genes. The genome of the model moss *Physcomitrium patens* harbors a relatively small number (49) of *PRX* genes. Conserved architecture of four exons and three '001' introns, found in some algal *PRX* genes and in the *PpPRX* family, suggests that this architecture predated divergence of the green algal and land plant lineages. The *PpPRX* family expanded mainly through whole-genome duplications. All duplicated pairs but one were under purifying selection and generally exhibited similar expression profiles. An expanded phylogenetic tree revealed a conserved land plant-wide clade that contained PRXs implicated in stress responses in non-lignifying cells, providing a clue to ancient functions of land plant PRXs. Functional clustering was not observed, suggesting convergent evolution of specific PRX functions (e.g., lignification) in different plant lineages. With its small complement of PRXs, *P. patens* may be useful for functional characterization of land plant PRXs. Several PpPRXs were proposed for further study, including *PpPRX34* and *PpPRX39* in the ancient land plant-wide clade.

Keywords: class III peroxidases; *Physcomitrium patens*; multigene family; gene duplication; expression profile; ancient enzyme functions

Citation: Aparato, V.P.M.; Rabbi, F.; Madarash, T.; Brisbourne, W.A.; Barker, E.I.; Suh, D.-Y. Genome-Wide Analysis of the Class III Peroxidase Gene Family in *Physcomitrium patens* and a Search for Clues to Ancient Class III Peroxidase Functions. *Int. J. Plant Biol.* **2024**, *15*, 1141–1161. https://doi.org/10.3390/ijpb15040079

Academic Editor: Alena Gajdošová

Received: 15 August 2024
Revised: 10 October 2024
Accepted: 18 October 2024
Published: 4 November 2024

1. Introduction

Peroxidases are a diverse group of enzymes that catalyze redox reactions in which substrates (e.g., monolignols) are oxidized while hydrogen peroxide (H_2O_2) or organic peroxides are reduced to water or corresponding alcohols. Based on the nature of the redox center, peroxidases are divided into heme or non-heme peroxidases [1]. Heme peroxidases are found in all kingdoms of life and comprise four superfamilies that evolved independently [2]. Among them, the peroxidase–catalase superfamily is currently the largest superfamily and is composed of three structurally distinct families, which are termed class I, II and III peroxidases [3]. Class I peroxidases are represented by ascorbate and cytochrome *c* peroxidases and their main function appears to be scavenging excess H_2O_2. Class II peroxidases include lignin-degrading fungal peroxidases (ligninases).

Secretory plant peroxidases such as horseradish peroxidases are categorized as class III peroxidases (PRXs). They are present as large multigene families in all land plants (embryophytes) and also in some streptophyte algae [4]. They are monomeric glycoproteins and are structurally characterized by four conserved disulfide bonds, two calcium ion binding sites, and an active site with a heme prosthetic group [5]. PRXs are secreted to the outside of the plant cell or to the vacuole and perform diverse tissue-specific functions. For example, PRXs oxidize substrates in lignification, suberization, and auxin catabolism.

They also generate or break down ROS (reactive oxygen species) in the processes of stress (e.g., pathogen) resistance, cell elongation, and germination [6,7]. A few examples of PRXs whose functions were studied by reverse genetics are as follows: *Arabidopsis* PRX2, PRX25, and PRX71 in lignification [8], a pepper PRX (CaPO2) in ROS generation and disease resistance [9], and *Arabidopsis* PRX16 in seed germination [10]. Due to their diverse roles in plant growth and development as well as in defense responses, *PRX* families have been identified and characterized in model plants or major crops, including *Arabidopsis* [11,12], rice [13], poplar [14], maize [15], pear [16], switchgrass [17], wheat [18], cotton [19], grapevine [20], potato [21], soybean [22], and tobacco [23].

Phylogenetic and gene network analyses have suggested that some PRXs likely emerged at the beginning of plant terrestrialization and that PRX families have expanded throughout plant evolution [24,25]. In turn, the antiquity and abundance of plant PRXs suggest that ancient plant PRXs may have played important roles in overcoming challenges encountered on land and, later, diversification of PRX functions may have helped plants to cope with increasing stresses during plant evolution. However, PRX families in vascular plants have a large number of members (e.g., 73 PRXs in *Arabidopsis* and 119 in maize) and their functional redundancy in addition to in vitro substrate promiscuity [17] make studying their contribution to plant terrestrialization and subsequent functional diversification difficult. Instead, PRX families of non-vascular plants with a smaller number of members can be advantageous in gaining insights to these questions [26].

Physcomitrium patens has emerged as a model moss [27]. Owing to the ease of transformation and vegetative propagation of transformed lines, gene knockout phenotypes can be readily screened [28]. Its genome sequence is well annotated, and large-scale tissue-specific gene expression data are available [29]. *P. patens* is also amenable to chemical rescue studies because its single cell layered tissues can uptake chemicals through the entire surface [30]. In line with its simple morphology and physiology, the number of *PRX* genes in *P. patens* is roughly half that in vascular plants. These characteristics make *P. patens* an excellent system for studying the functions and evolution of *PRX* genes with reverse genetics and chemical approaches. We are interested in how certain ancient PRXs contributed to the early evolution of land plants, especially in the metabolism of protective biopolymers (e.g., sporopollenin, lignin-like materials) and in spore development. In this study, we performed, for the first time for any bryophyte, a genome-wide analysis of the *PRX* gene family in *P. patens*. We identified forty-nine *PRX* genes and two pseudogenes and analyzed their deduced amino acid sequences, phylogeny, gene duplication events, and expression profiles. We also constructed large-scale phylogenetic trees in search of PRXs that are highly conserved in land plants and possibly possess ancient functions.

2. Materials and Methods

2.1. Identification and Sequence Analysis of Class III Peroxidase Genes in P. patens

P. patens PRX sequences collated in Lehtonen et al. [31] and in RedoxiBase (https://peroxibase.toulouse.inra.fr (accessed on 8 March 2023)) [32] were used for tBLASTn searches of the *P. patens* v3.3 genome in Phytozome 13 (https://phytozome-next.jgi.doe.gov (accessed on 8 March 2023)). Protein sequences of the candidate genes were further analyzed for the conserved amino acid residues [5] and named from PpPRX1 to PpPRX51 according to their chromosomal locations.

Subcellular localization was predicted using DeepLoc 2.0 (https://services.healthtech.dtu.dk/services/DeepLoc-2.0/ (accessed on 25 May 2023)) [33]. Transmembrane domains were predicted by Phobius, a combined transmembrane topology and signal peptide predictor (https://phobius.sbc.su.se/ (accessed on 25 May 2023)) [34]. Multiple sequence alignment was produced using the MAFFT L-INS-I method (https://mafft.cbrc.jp/alignment/server/ (accessed on 3 April 2024)).

2.2. Phylogenetic Analysis

A Maximum-Likelihood (ML) phylogenetic tree of the PpPRX family was reconstructed from amino acid sequences encoded by 49 *PpPRX* genes and 2 pseudogenes. The sequences were aligned using the MAFFT L-INS-I method and an ML tree was built in MEGA X [35] under the JTT substitution model. The initial tree was created using the default tree inference options. Support for the tree was measured using 1000 bootstrap replicates. The bootstrap consensus tree was then formatted using iTOL [36].

An ML tree of all PpPRXs and PRXs selected from eight model plants, each representing a major embryophyte lineage, was also reconstructed to find any embryophyte-spanning clades. Amino acid sequences of PRXs from *Anthoceros punctatus*, *Marchantia polymorpha*, *Selaginella moellendorffii*, *Ginkgo biloba*, *Amborella trichopoda*, *Oryza sativa*, and *Arabidopsis thaliana* were retrieved from RedoxiBase, and *Ceratopteris richardii* PRX sequences were obtained from Phytozome 13. Thirty-two non-redundant PRXs with reported functions (Table S1) were added to give a total of 855 PRXs (Table S2). APX1, an ascorbate peroxidase from *Arabidopsis*, was added to root the tree. The sequences were aligned in MAFFT and trimmed in AliView. An ML tree was reconstructed using the RAxML-HPC BlackBox tool in the CIPRES Gateway [37]. The WAG substitution model with the shape parameter of the gamma distribution, a proportion of invariable sites, and empirical amino acid frequencies was used (WAG + G + I + F). The number of discrete gamma categories was set to 4. Support for the tree was measured using bootstopping and clades with <50% support were collapsed into polytomies. Additionally, large algal or single-species clades were collapsed in iTOL and represented by black triangles.

2.3. Gene Duplication Analysis

Gene pairs were investigated for duplication events when two genes shared ≥70% protein sequence identity, or shared <70% sequence identity and had one or more companion gene pairs. Duplicated gene pairs were investigated for their phylogenetic relationship, Ka/Ks ratio, gene architecture, expression profile, and companion pairs in 50 kb flanking regions. In the lineage leading to *P. patens*, two whole-genome duplications (WGD) occurred [38]. In WGD1, seven ancestral (anc7) chromosomes were duplicated and subsequent loss of a chromosome resulted in thirteen (anc13) chromosomes. Following WGD2, fissions and fusions resulted in the extant twenty-seven chromosomes. A duplicated pair was assumed to be produced during WGD1 if the genes were located in two chromosomes that descended from the same anc7 chromosome but from different anc13 chromosomes. Similarly, a duplicated pair was assumed to be produced during WGD2 if the genes were present on two chromosomes that were descendants of the same anc13 chromosome. Two nearby duplicated genes were defined as tandemly duplicated (TD) genes when they were less than 100 kb apart and there were fewer than three intervening genes, or segmentally duplicated (SD) genes otherwise.

Ka and Ks values were obtained by first performing pairwise alignment of the coding region nucleotide sequences using MAFFT in RevTrans [39]. Each alignment was then imported into DnaSP v6 [40] to calculate asynonymous (Ka) and synonymous substitutions (Ks).

2.4. Gene Expression Analysis

P. patens developmental stage expression data were collated from the database PEAT-Moss [29]. To determine the number of clusters, wss and silhouette methods of *k*-means clustering were used where nstart was set at 25. Hierarchical clustering was calculated using the heatmap.2 package, employing the WardD2 and the Pearson correlation methods through R version 4.2.2. Gene and tissue dendrograms were generated using data obtained from Ortiz-Ramirez et al. [41]. The heatmap was generated from the same data using log2-transformed expression data in Microsoft Excel 2023.

3. Results

3.1. Identification and Sequence Analysis of PpPRXs

A total of 49 *PRX* genes and 2 pseudogenes were identified in the *P. patens* genome (Table 1). While most are single-copy genes, four genes have multiple copies and *PpPRX50* has four copies. *PpPRX49* and *PpPRX50* are reported here for the first time. To avoid misannotation of the other heme peroxidases that share parts of common PRX sequences [42], we used the following criteria:

1. Two signature sequences, RLxF<u>H</u>DC$_2$xxxGC$_3$DxS and LxGx<u>H</u>xxGxxxC$_6$, harboring the distal and proximal <u>H</u>is residues, respectively, of the heme (Figure S1) [13].
2. Eight conserved Cys (Cys1 to Cys8) that form four disulfide bonds.
3. Conserved residues at the two calcium binding sites, including Asp71, Asp78, and Ser80 for the distal site, and Ser195, Asp239, Thr242, and Asp247 for the proximal site (numbering of PpPRX1, Figure S1) [5].
4. Conserved gene architecture (intron locations and phases).
5. Signal peptide.

A few proteins were tentatively assigned to be PRXs, although they did not meet all the criteria. For example, PpPRX9 and PpPRX25 did not contain a predicted signal peptide, while PpPRX7 and PpPRX25 were predicted to be membrane-bound [43]. Several proteins, including PpPRX4 and PpPRX17, lacked one or two of the eight conserved Cys residues (Table 1). When two Cys residues were mutated, both were always a disulfide forming pair, such as Cys2 and Cys3 in PpPRX39, and Cys5 and Cys8 in PpPRX4, PpPRX25, PpPRX49, and PpPRX50. Hence, no PpPRX potentially lacking more than one disulfide bond was identified in this study. In an earlier study, a small fraction (<5%) of plant PRXs were predicted to lack one or two disulfide bonds [4].

Conserved residues in PpPRXs and in several PRXs from streptophyte algae and tracheophytes are highlighted in Figure S1.

There are four multicopy genes. *PpPRX2*, *PpPRX12*, and *PpPRX23* have two copies each, while 4 copies of *PpPRX50* are found. The lengths of untranslated regions that are identical in nucleotide sequence among gene copies are generally in the range of 700 to 2300 bp.

We also found two pseudogenes, ψPpPRX27 and ψPpPRX45 (Table 1). ψPpPRX27 suffered a nonsense mutation and two events of intron invasion. If it were expressed, a truncated polypeptide with 43 amino acid residues would be produced. ψPpPRX45 is a pseudogene with three nonsense mutations, and it would produce a truncated, 108 residue-long polypeptide.

Table 1. *P. patens PRX* genes and pseudogenes. Fifty-five *P. patens* genes and two pseudogenes are listed along with their identifiers, predicted subcellular localizations, and additional notes, including reported functions, predicted transmembrane domains, non-conservative amino acid substitutions, and other notable features.

Gene Name [a]	Gene ID (Phpat.)	Chromosome ID	RedoxiBase ID [b]	Subcellular Localization Prediction [c] (Probability)	Remarks
PpPRX1	001G073100	Pp3c1_19610	PpaPrx42	ExCel, 0.785	
PpPRX2A	002G117800	Pp3c2_28900	PpaPrx28	ExCel, 0.770	
PpPRX2B	002G118300	Pp3c2_28980	PpaPrx54	ExCel, 0.770	
PpPRX3	003G004400	Pp3c3_1110	PpaPrx38	Lys/Vac, 0.691	
PpPRX4	003G017700	Pp3c3_4040	PpaPrx29	ExCel, 0.661	Cys5→Ala [d]; Cys8→Val
PpPRX5	003G052800	Pp3c3_14160	PpaPrx07	ExCel, 0.772	
PpPRX6	003G083200	Pp3c3_21170	PpaPrx36	ExCel, 0.633	
PpPRX7	003G095600	Pp3c3_24230	PpaPrx16	ExCel, 0.654	TM domain predicted (12–29) [e]
PpPRX8	003G117800	Pp3c3_30190	PpaPrx08	ExCel, 0.816	Secreted in culture [f]
PpPRX9	003G136700	Pp3c3_34620	PpaPrx45		No signal peptide predicted

Table 1. *Cont.*

Gene Name [a]	Gene ID (Phpat.)	Chromosome ID	RedoxiBase ID [b]	Subcellular Localization Prediction [c] (Probability)	Remarks
PpPRX10	003G136800	Pp3c3_34630	PpaPrx46	ExCel, 0.806	
PpPRX11	004G003700	Pp3c4_1190	PpaPrx25	ExCel, 0.806	
PpPRX12A	004G052500	Pp3c4_14520	PpaPrx53	ExCel, 0.769	ROS production upon chitin treatment [g]; Found in rhizoid exudates [h]
PpPRX12B	004G052600	Pp3c4_14530	PpaPrx13	ExCel, 0.769	
PpPRX13	004G077800	Pp3c4_20300	PpaPrx15	ExCel, 0.897 Lys/Vac, 0.715	
PpPRX14	004G079600	Pp3c4_20640	PpaPrx10	Lys/Vac, 0.639	
PpPRX15	004G089100	Pp3c4_23370	PpaPrx44	ExCel, 0.623	
PpPRX16	004G089600	Pp3c4_23500	PpaPrx18	ExCel, 0.674	
PpPRX17	006G000100	Pp3c6_30	PpaPrx43	ExCel, 0.713	Cys2→Tyr; distal Phe→Tyr
PpPRX18	008G005700	Pp3c8_1520	PpaPrx47	ExCel, 0.767	
PpPRX19	008G022000	Pp3c8_5520	PpaPrx24	ExCel, 0.827	
PpPRX20	008G030400	Pp3c8_8070	PpaPrx34	ExCel, 0.717 Lys/Vac, 0.704	No intron
PpPRX21	008G039900	Pp3c8_11990	PpaPrx20	ExCel, 0.800 Lys/Vac, 0.591	
PpPRX22	008G048800	Pp3c8_14090	PpaPrx23	ExCel, 0.826 Lys/Vac, 0.612	
PpPRX23A	008G062400	Pp3c8_17000	PpaPrx52	ExCel, 0.754	
PpPRX23B	008G062600	Pp3c8_17040	PpaPrx06	ExCel, 0.754	
PpPRX24	009G071300	Pp3c9_18550	PpaPrx11	ExCel, 0.663 Lys/Vac, 0.635	
PpPRX25	010G064700	Pp3c10_16840	PpaPrx31		TM domain predicted (6–28) [e]; Cys5→Ala; Cys8→Ile; Ca^{2+}-binding Ser→Phe
PpPRX26	010G078500	Pp3c10_20710	PpaPrx03	ExCel, 0.700 Lys/Vac, 0.647	Secreted in culture [f]
ψPpPRX27		Pp3c11_4960			A nonsense mutation; highly similar to PpPRX12 and PpPRX17
PpPRX28	012G019000	Pp3c12_5770	PpaPrx26	ExCel, 0.800	
PpPRX29	012G021500	Pp3c12_6740	PpaPrx41	ExCel, 0.816 Lys/Vac, 0.707	
PpPRX30	012G060400	Pp3c12_16500	PpaPrx27	ExCel, 0.672	
PpPRX31	012G069400	Pp3c12_19290	PpaPrx02	ExCel, 0.620	
PpPRX32	013G005500	Pp3c13_1880	PpaPrx22	ExCel, 0.650 Lys/Vac, 0.671	
PpPRX33		Pp3c13_23840	PpaPrx33	ExCel, 0.640 Lys/Vac, 0.587	
PpPRX34	015G054100	Pp3c15_13950	PpaPrx01	ExCel, 0.716 Lys/Vac, 0.590	
PpPRX35	015G083400	Pp3c15_22510	PpaPrx17	ExCel, 0.787	Secreted in culture [f]
PpPRX36	016G078100	Pp3c16_18920	PpaPrx35	ExCel, 0.723	Cys6→Trp; distal Phe→Tyr
PpPRX37	017G020300	Pp3c17_6050	PpaPrx39	ExCel, 0.688 Lys/Vac, 0.610	
PpPRX38	019G055400	Pp3c19_16160	PpaPrx04	ExCel, 0.628	Secreted in culture [f]
PpPRX39	019G071300	Pp3c19_20780	PpaPrx05	ExCel, 0.752	Cys2→Phe; Cys3→Ala; distal Asn→Met
PpPRX40	020G057600	Pp3c20_15730	PpaPrx21	ExCel, 0.805	Secreted in culture [f]
PpPRX41	022G030300	Pp3c22_8030	PpaPrx48	ExCel, 0.839	
PpPRX42	023G023800	Pp3c23_8110	PpaPrx12	ExCel, 0.787	
PpPRX43		Pp3c24_10570	PpaPrx30	ExCel, 0.732	
PpPRX44	024G055300	Pp3c24_15170	PpaPrx32	ExCel, 0.845 Lys/Vac, 0.662	
ψPpPRX45		Pp3c24_17400			3 nonsense mutations; highly similar to PpPRX23
PpPRX46	026G012400	Pp3c26_2960	PpaPrx14	ExCel, 0.707 Lys/Vac, 0.607	Cys8→Met
PpPRX47	026G012800	Pp3c26_3070	PpaPrx19	ExCel, 0.783	Upregulated on salt and H_2O_2 treatments [i]

Table 1. *Cont.*

Gene Name [a]	Gene ID (Phpat.)	Chromosome ID	RedoxiBase ID [b]	Subcellular Localization Prediction [c] (Probability)	Remarks
PpPRX48	026G012900	Pp3c26_3080	PpaPrx09	ExCel, 0.800	
PpPRX49	026G021400	Pp3c26_5480		ExCel, 0.685	Cys5→Ala; Cys8→Phe
PpPRX50A	026G021900	Pp3c26_5670		ExCel, 0.682	Cys5→Ala; Cys8→Phe
PpPRX50B	026G022100	Pp3c26_5720		ExCel, 0.682	Cys5→Ala; Cys8→Phe
PpPRX50C	026G022300	Pp3c26_5800		ExCel, 0.682	Cys5→Ala; Cys8→Phe
PpPRX50D	026G022400	Pp3c26_5840		ExCel, 0.682	Cys5→Ala; Cys8→Phe
PpPRX51	026G023700	Pp3c26_6390	PpaPrx37	ExCel, 0.897	Cys1→Ser

[a] New nomenclature is based on chromosomal locations from lowest chromosome and lowest nucleotide to the highest of each. [b] https://peroxibase.toulouse.inra.fr/ (accessed on 8 March 2023). [c] DeepLoc 2.0 (https://services.healthtech.dtu.dk/services/DeepLoc-2.0 (accessed on 25 May 2023)). Probability values that are above thresholds are shown. ExCel, extracellular; Lys/Vac, lysosome/vacuole. [d] Mutation of the fifth Cys (Cys5) to Ala. Eight conserved Cys residues that form disulfide bonds are numbered from the N-terminus. See also Figure S1. [e] Transmembrane (TM) domain was predicted by Phobius (https://phobius.sbc.su.se/ (accessed on 25 May 2023)). TM domains with a posterior probability higher than 0.5 are reported. The numbers in parentheses indicate amino acid residue numbers the domain was predicted to span. [f] Lehtonen et al. (2014) [44]. [g] Lehtonen et al. (2012) [45]. [h] Martinez-Cortes et al. (2014) [46]. [i] Martinez-Cortes et al. (2021) [47].

3.2. Phylogenetic Analysis of the PpPRX Family

The rooted ML tree of PpPRX sequences comprised seven major clades, A to F, and clades C and F were further divided into multiple subclades (Figure 1). Except for the singleton clade C1 (PpPRX41), all nodes were supported by bootstrap values higher than 50%. The seven major clades were hierarchical: clade A of PpPRX34 and PpPRX39 was sister to the rest of the family, while clade B was sister to clades C–F. Clade D consisted of a single gene, PRX30, sister to clades E and F.

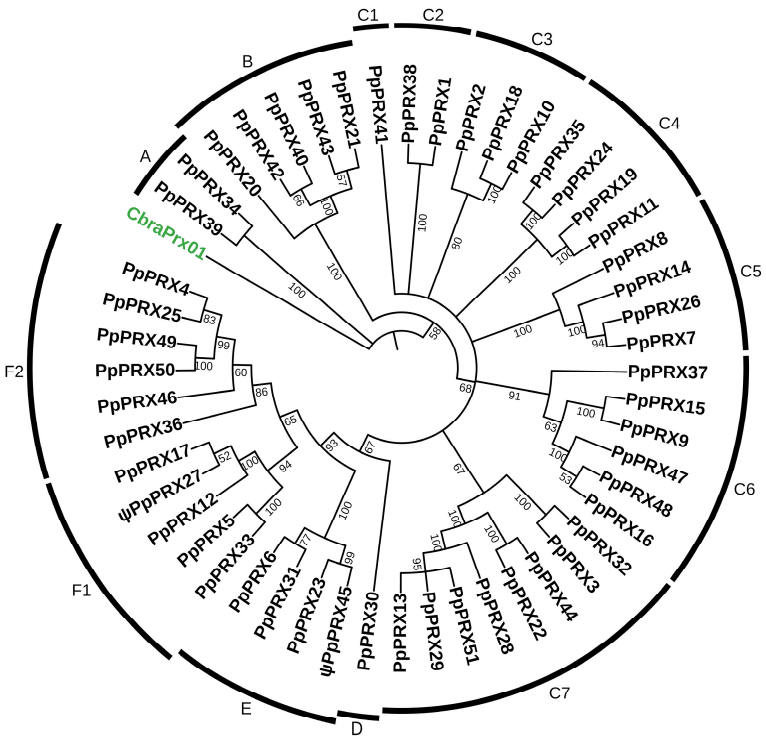

Figure 1. Maximum-Likelihood phylogenetic tree of *P. patens* PRX family.

A Maximum-Likelihood tree was constructed in MEGA X with the JTT substitution model and rooted with an algal PRX sequence from *Chara braunii* (CbraPrx01, GenBank accession id, GBG90290.1). Numerical values at nodes indicate bootstrap support above 50% from 1000 bootstrap replicates. Clades of the same phylogenetic level are labeled from A to F and sister clades within each level are labeled numerically.

3.3. Gene Architecture

Of 49 *PpPRX* genes, 18 genes have three introns at conserved positions (Figures 2 and S1). Introns 1 and 2 are phase 0 introns, while intron 3 is a phase 1 intron. As shown in Figure 2, these '001' introns are not only highly conserved in plant *PRX* genes (e.g., horseradish *PRX C1*), but also are found in some streptophyte algal genes (e.g., *Klebsormidium nitens PRX* and *Spirogyra* sp. *PRX03*). Intron 1 is positioned between Cys2 and Cys3, downstream of the distal His residue, while intron 3 is positioned upstream of the proximal His residue (Figure S1). The other 27 *PpPRX* genes experienced at least one intron loss, whereas four genes (*PRX11*, *PRX22*, *PRX44*, *PRX25*) underwent intron loss and gain events (Figure 2).

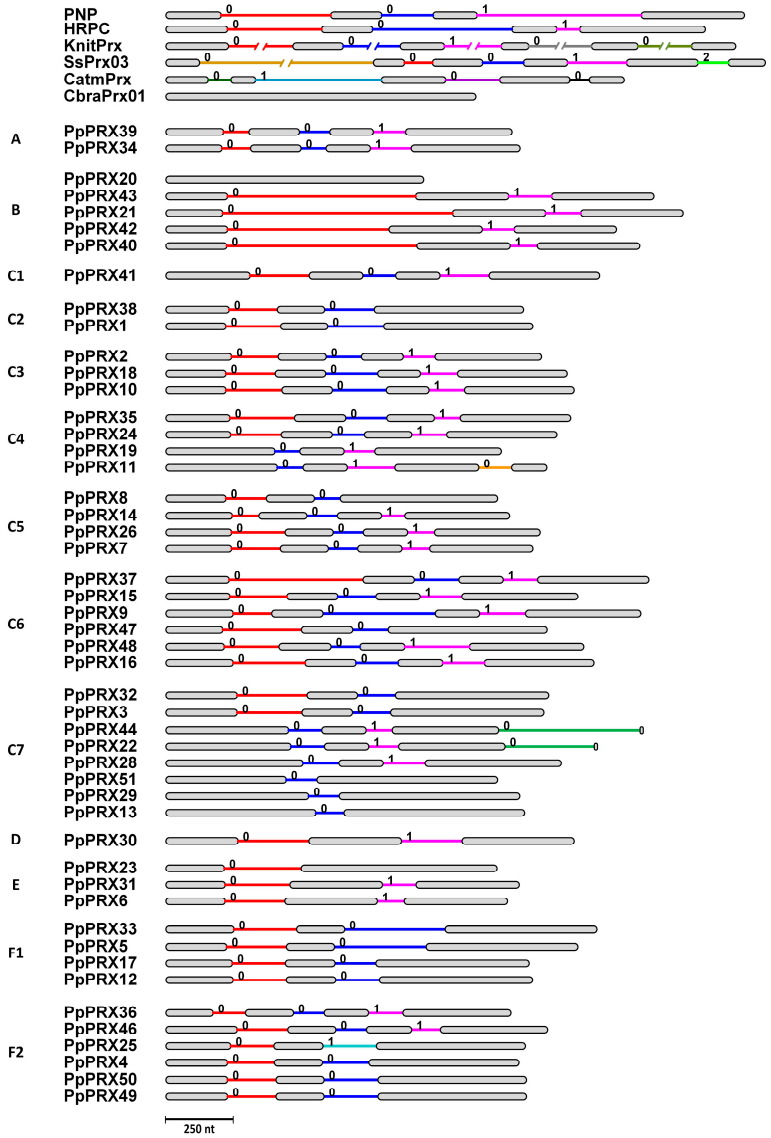

Figure 2. Architecture of *P. patens PRX* genes and conservation of their intron positions and phases. Each gene is represented by gray bars (exons) and colored lines (introns), and the number above each intron is its intron phase. Three highly conserved introns in plant *PRX* genes as identified by Mathé et al. (2010) [48] are shown in red, blue, and pink, respectively. Non-conserved introns that are found in certain genes are shown in other colors, e.g., brown in *PpPRX11*. *PpPRX* genes are grouped according to clade in the Maximum-Likelihood phylogenetic tree (Figure 2). Architecture of *PRX* genes from vascular plants and algae are given for comparison. PNP, peanut *PRX1*; HRPC, horseradish isozyme C1; KnitPrx, *Klebsormidium nitens PRX*; SsPrx03, *Spirogyra* sp. *PRX03*; CatmPrx, *Chlorokybus atmophyticus PRX*; CbraPrx01, *Chara braunii PRX01*.

In general, *PpPRX* genes in the same phylogenetic clade share identical gene architecture. For example, *PpPRX* genes in clade C6 share the conserved '001' introns except for *PpPRX47* that lost intron 3. All four *PpPRX* genes in clade F1 lost intron 3 (Figure 1).

Gene architecture was identical in each pair of sister genes at the tip of the tree (e.g., *PpPRX34–PpPRX39*, *PpPRX40–PpPRX42*, etc.). One notable exception was the *PpPRX11–PpPRX19* pair in clade C4, as PpPRX11 gained an intron in exon 3.

3.4. Chromosomal Locations and Gene Duplications

In Figure 3, the evolutionary history of the 27 extant chromosomes is illustrated using colors and shades, as in Lang et al. [38]. Forty-nine *PpPRX* genes and two pseudogenes were distributed unevenly among the chromosomes. Chromosomes 3 and 26 harbored the most genes (8 and 6, respectively), while seven chromosomes had none. Seven descendants of one particular anc7 chromosome (green shades in Figure 3) were disproportionally populated as a total of 30 genes were located on them, many of them in tandem arrays.

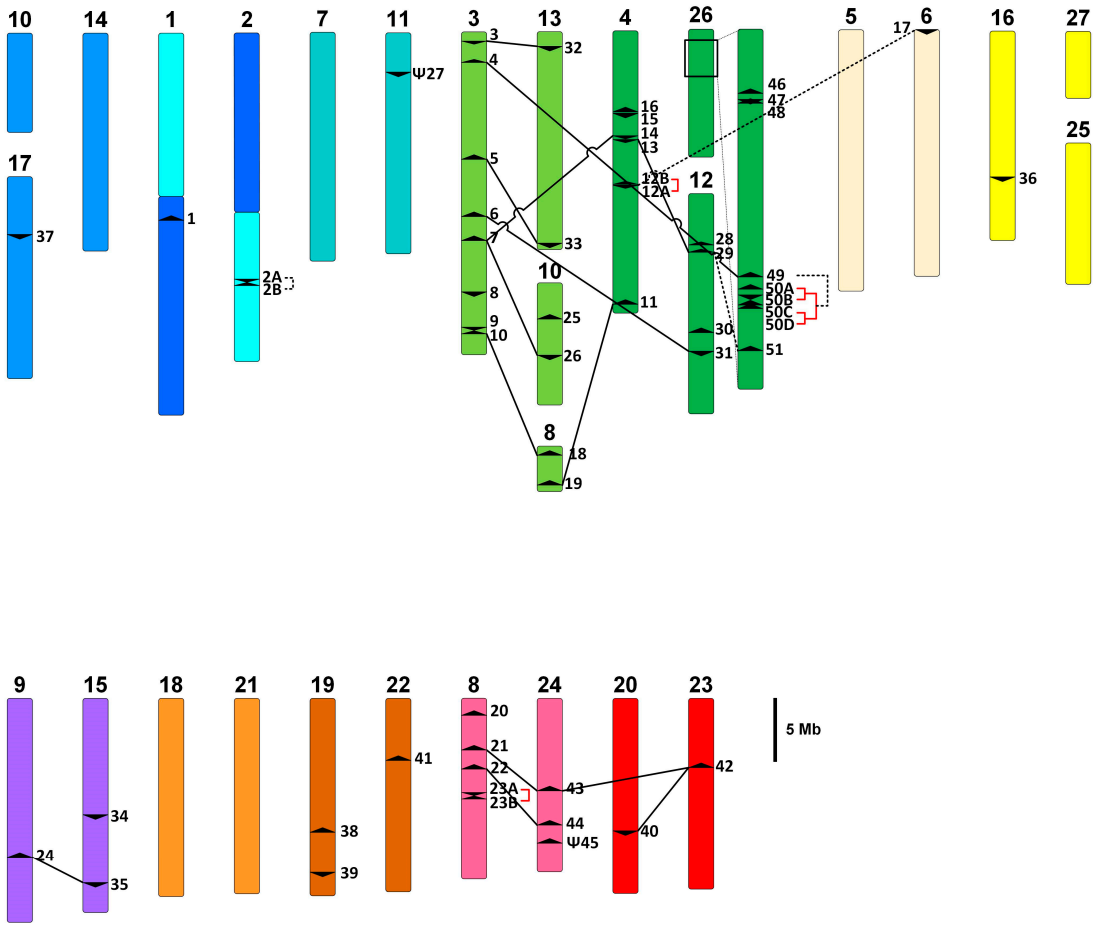

Figure 3. Chromosomal locations of *P. patens PRX* genes and proposed duplication pairs. A scale diagram of the *P. patens* genome was adapted from Figure 5c in Lang et al. (2018) [38]. Colors and shades of chromosomes reflect the evolution of the genome from seven ancestor (anc7) chromosomes through two WGDs and chromosomal fission or fusion events. For example, the extant chromosomes 3, 13, 10, 8, 4, 26, and 12, all in different shades of green, are descendants of one of the anc7 chromosomes, while chromosomes 5, 6, 16, 27, and 25, all in different shades of yellow, are descendants of another anc7 chromosome, and so on (for details, refer to Figure 5c in Lang et al., 2008) [38]. The location of each *PpPRX* gene was marked with arrowheads depicting forward or reverse orientation of the gene. Tandem duplications were depicted by red square brackets, segmental duplications by broken black lines, and WGDs by solid black lines. Sections of chr8 and chr26 were zoomed in for clarity.

A total of 22 duplication pairs were further analyzed (Table 2). Four genes in clade B of the ML phylogenetic tree (Figure 1) were descendants of a single ancestral gene that was present on the red anc7 chromosome. A plausible scenario was as follows. An ancestral gene was duplicated in WGD1 to give the *PpPRX42–PpPRX43* pair. Each gene was once again duplicated in WGD2 to give the *PpPRX40–PpPRX42* and *PpPRX21–PpPRX43* pairs. Two companion gene pairs duplicated during WGD1 were found in the immediate vicinity (<50 kb) of the *PpPRX42–PpPRX43* pair. They were a pair of putative *STRUCTURAL MAINTENANCE OF CHROMOSOMES* genes (Pp3c23_8100 and Pp3c24_10590) and a pair of genes encoding putative glyceraldehyde-3-phosphate dehydrogenases (Pp3c23_8160 and Pp3c24_10620) (Table 2). Similarly, at least one companion gene pair was found for four other WGD pairs. *PpPRX2A* and *PpPRX2B*, the two copies of *PpPRX2* with identical nucleotide sequences, also had a companion gene pair and were therefore considered segmental duplicates. Interestingly, the companion pair, Pp3c2_28870 and Pp3c2_29010, had only 61% nucleotide sequence identity. Other gene copies were products of tandem duplications (TD).

All duplication pairs have been under purifying selection (Ka/Ks < 1), except *PpPRX49–PpPRX50*, whose Ka/Ks value of 1.024 suggested neutral selection (Table 2).

Although not included in our detailed analysis due to their ≤70% sequence identity, seven more gene pairs were considered to be possible duplicated pairs. The gene pairs, their clade name (Figure 1), sequence identity (%), and mode of duplication are as follows: *PpPRX1–PpPRX38* (clade C2, 62.8%, segmental duplication (SD)), *PpPRX4–PpPRX25* (clade F2, 64.9%, WGD2), *PpPRX9–PpPRX15* (clade C6, 57.1%, WGD1), *PpPRX16–PpPRX48* (clade C6, 62.7%, WGD2), *PpPRX20–PpPRX21* (clade B, 67.5%, SD), *PpPRX20–PpPRX34* (clades B–A, 61.0%, SD), *PpPRX34–PpPRX39* (clade A, 59.1%, SD).

3.5. Gene Expression Profile

Expression data of *PpPRX* genes from different moss tissues reported by Ortiz-Ramírez et al. [41] are presented in Figure 4. Expression data from comparable tissues from other datasets accessible in PEATMoss were in general agreement. To support the large-scale data collated in PEATMoss, we also performed RT-PCR to study tissue-specific expression of three select PpPRX genes (*PpPRX7*, *PpPRX9*, and *PpPRX32*) (Figure S2). In agreement with the data shown in Figure 4, *PpPRX7*, *PpPRX9*, and *PpPRX32* were most highly expressed in young green sporophytes. Particularly, *PpPRX9* was almost exclusively expressed in green sporophytes.

As shown in the dendrogram above the heatmap in Figure 4, expression profiles of *PpPRX* genes in different tissues were grouped into two clusters. One cluster comprised archegonia, developing green (S1, S2, S3) sporophytes and gametophores, and the other cluster comprised chloronemata, caulonemata, rhizoids, mature brown sporophytes, and spores. *PpPRX* genes were also grouped into two gene clusters according to their expression profiles, as shown in the gene dendrogram on the left side of the heatmap. Most genes in cluster A were relatively highly expressed in archegonia, green sporophytes, and gametophores, while most genes in cluster B were relatively highly expressed in rhizoids, protonemata, or spores. Expression levels are reported here as high (>3.1), moderate (−3.6 to 3.1), or low ≤ −3.6), the top, middle, and bottom tertiles, respectively.

Table 2. Duplication pairs of *P. patens PRX* genes. Duplication pairs from *P. patens* PRX genes are listed according to their phylogenetic clade. Their duplication type, amino acid sequence identity, Ka/Ks ratio, exon–intron architecture conservation, and companion gene pairs are listed. Their expression profiles are also compared.

Clade [a]	Duplicated Gene Pairs	Duplication Type [b]	%Identity [c]	Ka	Ks	Ka/Ks	Exon/Intron Architecture	Expression Profiles [d]	Companion Gene Pairs [e]
B	*PpPRX42–PpPRX43*	WGD1	71.7	0.184	1.446	0.127	Conserved	AIa–AIb	Pp3c23_8100–Pp3c24_10590 Pp3c23_8160–Pp3c24_10620
	PpPRX21–PpPRX43	WGD2	78.8	0.109	0.813	0.134	Conserved	AIa–AIb	
	PpPRX40–PpPRX42	WGD2	81.6	0.107	0.836	0.127	Conserved	AIa–AIa	
C3	*PpPRX10–PpPRX18*	WGD2	75.5	0.159	0.608	0.261	Conserved	AII–BIa	
	PpPRX2A–PpPRX2B	SD	100				Conserved		Pp3c2_28870–Pp3c2_29010
C4	*PpPRX11–PpPRX19*	WGD1	71.8	0.164	2.832	0.058	Intron gain in PpPRX11	AIa–AIb	
	PpPRX24–PpPRX35	WGD2	75.1	0.169	1.751	0.097	Conserved	AIa–AIa	
C5	*PpPRX7–PpPRX14*	WGD1	63.4	0.275	1.393	0.197	Conserved	AIb–AIb	Pp3c3_24110–Pp3c4_20580 Pp3c3_24250–Pp3c4_20710
	PpPRX7–PpPRX26	WGD2	75.3	0.170	0.887	0.192	Conserved	AIb–AIa	Pp3c3_24110–Pp3c10_20720 Pp3c3_24130–Pp3c10_20740 Pp3c3_24250–Pp3c10_20630
C7	*PpPRX3–PpPRX32*	WGD2	81.6	0.107	0.695	0.154	Conserved	AIa–AIa	Pp3c3_1090–Pp3c13_1900 Pp3c3_1160–Pp3c13_1740
	PpPRX22–PpPRX44	WGD2	80.7	0.119	1.270	0.094	Conserved	BIb–BIIa	
	PpPRX13–PpPRX29	WGD2	75.8	0.136	1.028	0.133	Conserved	BIb–BIa	
	PpPRX29–PpPRX51	SD	72.1	0.158	0.984	0.161	Conserved	BIa–BIIb	
E	*PpPRX6–PpPRX31*	WGD1	59.4	0.332	1.362	0.243	Conserved	BIIb–BIb	Pp3c3_21160–Pp3c12_19360
	PpPRX23A–PpPRX23B	TD	100				Conserved		
F1	*PpPRX5–PpPRX33*	WGD2	72.4	0.169	0.840	0.199	Conserved	BIIa–BIIa	
	PpPRX12–PpPRX17	SD	83.3	0.089	0.232	0.381	Conserved	BIIa–AIa	
	PpPRX12A–PpPRX12B	TD	100				Conserved		
F2	*PpPRX4–PpPRX49*	WGD1	77.1	0.139	0.360	0.386	Conserved		
	PpPRX49–PpPRX50	SD	99.7	0.0042	0.0041	1.024	Conserved		
	PpPTX50A–PpPRX50B	TD	100				Conserved		
	PpPTX50C–PpPRX50D	TD	100				Conserved		

[a] Clade nomenclature according to Figure 1. [b] SD, segmental duplication; TD, tandem duplication; WGD1, the first whole-genome duplication; WGD2, the second whole-genome duplication. [c] Amino acid sequence identity was obtained using MatGAT (https://www.angelfire.com/nj2/arabidopsis/MatGAT.html (accessed on 3 April 2023)). [d] Expression profile clusters of duplicates from the gene dendrogram in Figure 4 are given. [e] Companion gene pairs that duplicated together in SD were searched within 50 kb in both directions of each duplicated *PpPRX* gene.

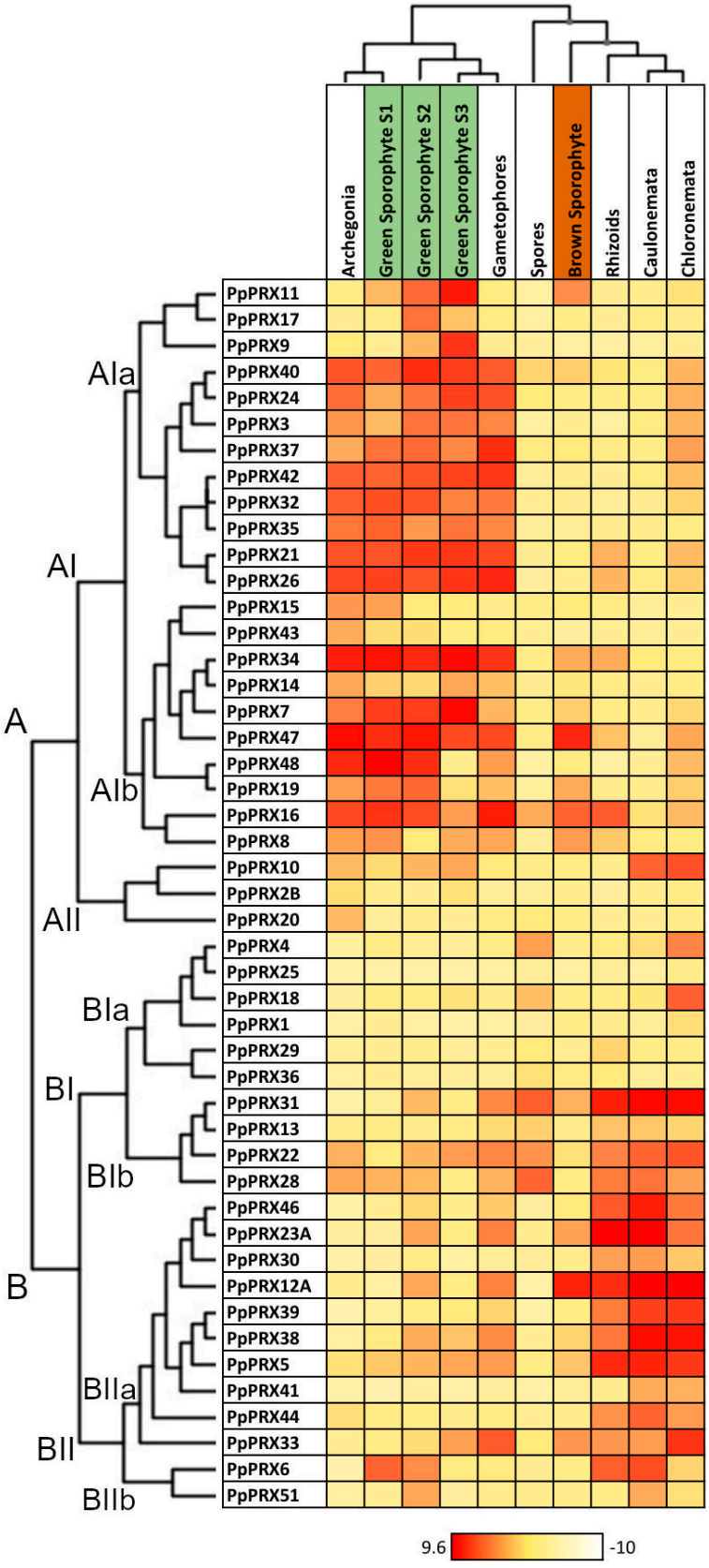

Figure 4. Heatmap of *P. patens PRX* gene expression. Expression values of *P. patens PRX* genes in each reproductive stage are represented by the color gradient from white to red. Dendrograms show groupings of genes or tissues with similar expression patterns. The heatmap was created from log2-transformed NimbleGen microarray data from Ortiz-Ramirez et al. [41].

Different *PpPRX* genes exhibited distinct tissue expression profiles. No gene exhibited either high or low expression in all tissues. A few genes were highly expressed in a relatively wide range of tissues. *PpPRX47* exhibited high expression in all tissues except spores and caulonemata, *PpPRX16* except in caulonemata, *PpPRX22* except in S1 green and mature brown sporophytes, *PpPRX28* except in S3 green and mature brown sporophytes, and PpPRX5 except in archegonia and spores. Certain genes were highly expressed in only a few particular tissues. *PpPRX9* and *PpPRX17* were expressed highly only in S2 and S3 green sporophytes, *PpPRX15* and *PpPRX20* in archegonia and S1 green sporophytes, *PpPRX43* in S1 green sporophytes, *PpPRX4* and *PpPRX18* in spores and chloronemata, *PpPRX41* in protonemata, *PpPRX44* in rhizoids and protonemata, and *PpPRX51* in S2 green sporophytes and caulonemata.

Duplicated gene pairs generally exhibited similar expression profiles. For example, *PpPRX40–PpPRX42*, *PpPRX24–PpPRX35*, and *PpPRX3–PpPRX32*, all WGD2 duplicated pairs, belonged to gene cluster AIa and were expressed highly in archegonia, sporophytes, and gametophores. There were exceptions. While *PpPRX10* of gene cluster AII was highly expressed in sporophytes and protonemata, its duplicate PpPRX18 belonged to cluster BIa and was expressed highly in spores and chloronemata. Also, PpPRX12 and its segmental duplicate PpPRX17 showed distinct expression profiles (Table 2).

3.6. Phylogenetic Analysis of Embryophyte PRX Sequences

Diverse *in planta* functions reported for 62 embryophyte PRXs were grouped into five broad categories, including lignin metabolism and ROS production/oxidative burst (Table S1). An ML tree of 855 PRXs comprising (1) 62 PRXs with reported *in planta* functions, (2) all PRXs from the fully sequenced genomes of eight plant species representing major embryophyte lineages, and (3) all PpPRXs is shown in Figure 5.

First, little clustering of the reported PRX functions was observed. PRXs with lignin metabolizing activity were found scattered in most major clades. Likewise, PRXs with ROS-related activities were present in multiple clades. Local clustering of putative orthologues or paralogues was also observed. AtPRX40, GhPOD, and ppa008309m, all implicated in male reproductive processes, were found in a tip clade together, while LePrx09, CsPRX25, and TaPRX-2A, all implicated in stress response, were also found closely clustered (Figure 5).

Second, one clade was found to contain PRX sequences from *P. patens* and each of the other eight lineage-representing species included in the tree reconstruction. This land plant-wide clade (yellow-shaded in Figure 5) contained seven PpPRXs. PpPRX34 and PpPRX39, which were in the early divergent clade A in the PpPRX ML tree, were also found in this 'land plant-wide clade', along with the five PpPRXs in clade B (Figure 1).

Also found in the clade were three angiosperm PRXs with reported functions: poplar PrtPO21 and tobacco TP60, both with lignin polymerization activity, and tomato LePrx17 involved in pathogen defense (Table S1 and references therein). OsPPX73, OsPRX116, and AtPRX42 had previously been reported as candidate ancient PRXs in rice and *Arabidopsis*, respectively [11,13] (see Section 4).

Third, there were taxa-specific clades: three tracheophyte-specific clades (shaded in gray) were found in the tree. Other clades contained PRXs from most plant species, but lacked PRXs from a few species, suggesting lineage-specific gene losses.

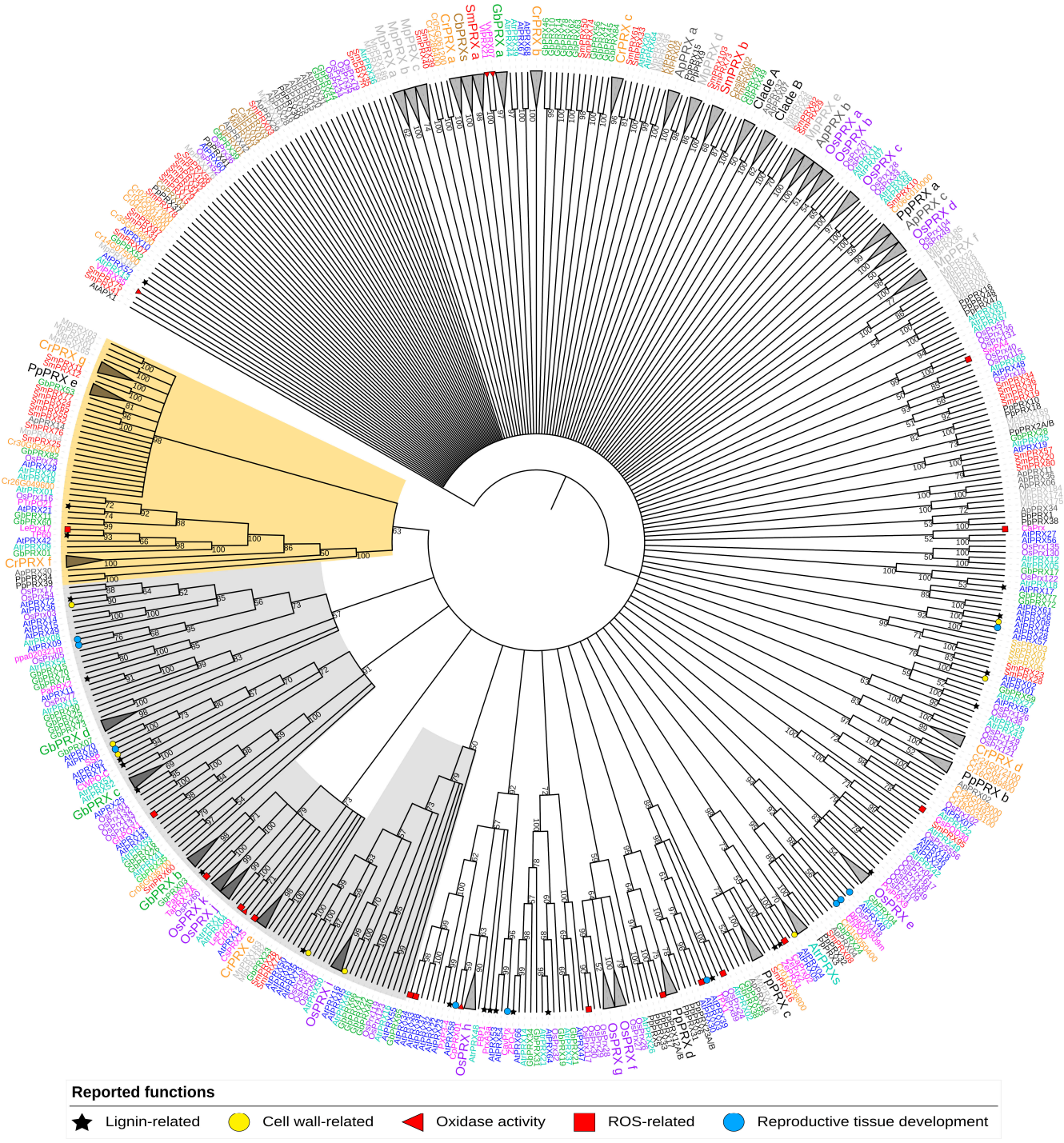

Figure 5. Maximum-Likelihood phylogenetic tree of selected embryophyte peroxidases. The tree, consisting of all PRX sequences from *Anthocerus punctatus* (ApPRX, dark grey), *Marchantia polymorpha* (MpPRX, light grey), *Selaginella moellendorffii* (SmPRX, red), *Ceratopteris richardii* (orange), *Ginkgo biloba* (GbPRX, green), *Amborella trichopoda* (AtrPRX, teal), *Oryza sativa* (OsPRX, purple), *Arabidopsis thaliana* (AtPRX, blue), *P. patens* (PpPRX, black), and PRXs with reported functions (pink), was constructed using the WAG + G + I + F substitution model for amino acids and rooted with APX1, an ascorbate peroxidase from *Arabidopsis*. Values at each node represent bootstrap support above 50%. The clade shaded in yellow represents an embryophyte-spanning clade, while the gray-shaded clades are tracheophyte-specific. *In planta* functions, grouped in five common categories (Table S1), are indicated with different symbols. Gene IDs and sequences of PRXs from the streptophyte algal species and eight plant species in the tree are provided in Table S2.

4. Discussion

4.1. With Conserved Characteristics and Relatively Fewer Genes, the PpPRX Family Is a Good Model for Further Study

Amino acid residues characteristic of PRX proteins at the heme-binding site and two Ca^{2+}-binding sites were highly conserved in all 49 PpPRXs. A total of nine PpPRXs are predicted to lack one of the four conserved disulfide bonds. This is not unusual. However, the frequency of mutation (9 of 49, 18%) was higher than the <5% reported by Mbadinga Mbadinga et al. [4], who counted 41 PRXs missing at least one Cys residue out of 959 PRXs analyzed. The disulfide bond Cys6–Cys7 is close to the substrate binding channel and may affect substrate selectivity [48]. PpPRX36, which is a singleton in clade F2 in the ML tree of the PpPRX family (Figure 1) and is expressed moderately across the tissues (Figure 4), is the only one with a mutation of Cys6.

Gene architecture of four exons and three '001' introns has been widely conserved in embryophyte *PRX* genes and it was suggested that this intron pattern was established in the last common ancestor of embryophytes [18]. Our finding of the same intron patterns in some streptophyte algal *PRX* genes (Figure 2) suggested that this particular *PRX* gene architecture was already present in the common ancestor of the streptophyte algal and embryophyte lineages. Intron loss was more frequent than intron gain during plant evolution [49]. Similarly, there were more intron losses than gains in *PpPRX* genes.

In this study, we examined all genes annotated as class III PpPRXs in the databases to select 49 *PRX* genes, including two *PRX* genes that have not been reported previously. Due to the stringent criteria we employed, the total number is less than what has been reported in the literature (e.g., 57 *PpPRX* genes in Mbadinga Mbadinga et al. [4]; 60 in Yan et al. [18]). In addition to the two pseudogenes (Table 1), we found five gene fragments that would produce short proteins of 86 to 177 amino acid residues (Pp3c4_8630, Pp3c15_15230, Pp3c20_5210, Pp3c20_5220, Pp3c23_3415). Due to massive and recent duplications, *PRX* families in vascular plants are larger; there are 73 *PRX* genes in *Arabidopsis*, 93 in poplar, 102 in potato, and 119 in maize. The large number of genes and high functional redundancy in vascular plants make it challenging to study the functions of tracheophyte *PRX* genes [6]. With its smaller size, the *PpPRX* family may serve as a model system for functional studies of plant *PRX* genes.

4.2. The PpPRX Family Expanded Mainly Through Whole-Genome Duplications

Among the 18 non-tandem duplications observed in the *PpPRX* family, 14 were attributed to WGDs and 4 to SD (Table 2). There were only four TDs, accounting for 18% (4 of 22) of total duplication events. This was in sharp contrast to the larger contribution of TD in the expansion of vascular plant *PRX* families. There were 57 SD and 26 TD events in potato, and 16 SD and 12 TD events in maize. In the model C4 grass *Setaria viridis*, 70% of *PRX* genes, 108 of 154 genes, were produced through TD events [50]. It was argued that genes encoding proteins that are more loosely connected in a network, such as *PRX* and others involved in stress responses in plants, are less restricted by gene dosage effects and hence would be retained more frequently after TD events. For example, the poplar vacuole *PRX* genes expanded by TD ([14], and references therein). The biological significance of the relative rarity of TD events in the *PpPRX* family is unclear.

Duplication mode affects divergence of expression profile. In *Arabidopsis*, poplar, and pear, genes produced through WGD were found to exhibit a lower divergence of expression profile than other duplicated genes [51–53]. This may explain why most WGD-produced *PpPRX* genes showed similar expression profiles.

Purifying selection has been a common feature in the evolution of plant *PRX* genes. Duplicated *PRX* genes in maize [15], pear [16], *Brachypodium distachyon* [54], grapevine [20], carrot [55], birch [56], tobacco [23], and cotton [19] were all predominantly subjected to purifying selection, indicating that the gene family has undergone relatively conservative evolution with stable structure and function. The *PpPRX* family was not an exception and all duplicated pairs but one were subject to negative selection.

4.3. Searching for Ancient and Conserved PRX Functions

PRX genes were first thought to have evolved in the lineage leading to land plants (embryophytes) and researchers have long sought to learn how ancestral *PRX* genes may have facilitated terrestrialization of ancient plants. It was speculated that ancient *PRX* genes might have functioned to mitigate UV-induced oxidative stresses or to contribute to formation of novel cell wall structures [13].

The single embryophyte-wide clade in our phylogenetic tree (Figure 5) included two moss sequences, PRX34 and PRX39. OsPRX73 and OsPRX116 had already been shown to be phylogenetically closer to a liverwort PRX than to any other rice PRX [13]. Likewise, the sequence of AtPRX42 was found to be ~80% identical to those of PRXs from cotton, soybean, and tobacco and 57% identical to its closest paralog, AtPRX21. AtPRX42 and AtPRX21 were suggested to have conserved the sequence and function of an ancestral embryophyte PRX gene [11,57]. We found that PpPRX34 and PpPRX39 were 42% and 36% identical, respectively, to AtPRX42. That is, AtPRX42 showed higher % identity to its *P. patens* orthologues than to any other AtPRX except AtPRX21.

AtPRX42 (At4g21960) and *AtPRX21* (At2g37130) are constitutively expressed in all tissues examined, including 2-day-old germinating seeds [57,58]. A recent study showed that AtPRX42, one of the most predominant AtPRXs in the *Arabidopsis* stem, was localized in non-lignifying xylem parenchyma and phloem cells and proposed to be involved in various stress responses [59]. This agreed remarkably well with the functions proposed by Passardi et al. [13] for ancient PRXs: protection of primary cell walls from oxidative stresses. We were not able to find any functional study of OsPRX73 (LOC_Os05g14260) and OsPRX116 (LOC_Os07g49360). Both genes were annotated as 'Stress Response' (GO:0006950) genes in the Rice Genome Annotation Project (http://rice.uga.edu/ (accessed on 28 August 2023)). *OsPRX73* is expressed at low levels in anther, leaf, panicle, root, seed, and shoot, while *OsPRX116* is expressed at a high level in panicle and moderately in leaf, root, seed, and shoot (http://expression.ic4r.org/ (accessed on 28 August 2023)). Interestingly, the two *PpPRX* genes in the clade showed expression profiles that are complementary, suggesting subfunctionalization of the genes after duplication. *PpPRX34* of expression cluster AIb (Figure 4) was highly expressed in archegonia, sporophytes, and gametophores, whereas *PpPRX39* of BIIa was mainly expressed in rhizoids and protonemata.

The land plant-wide clade in the ML tree (Figure 5) is by no means complete. Further studies with more sequences from diverse taxa and their functional characterization will be required. Current data suggested that stress response was the main function of ancient and conserved PRXs in the land plant-wide clade and gene duplications and subfunctionalization (OsPRX73 and OsPRX116) or neofunctionalization (TP60 and PrtPO21 in lignification) subsequently occurred in different lineages. In *P. patens*, at least six duplications occurred to create the seven PpPRXs in the clade. Functional studies on some of these PRXs should be informative.

4.4. Candidate PpPRX Genes for Future Studies

PRX can oxidize a variety of substrates or generate ROS *in planta*, and exhibits substrate promiscuity in vitro [60]. In addition, functional redundancy and compensation among *PRX* genes have made it difficult to study the biological functions of individual *PRX* genes. It has also been difficult to predict PRX functions based on sequence similarity and phylogeny [6,48]. This is partly due to functional divergence of duplicated genes as in the case of *AtPRX72* in lignification and *AtPRX36* in cell wall loosening and seed germination (Figure 5; Table S1). Further, some PRX functions (e.g., lignin polymerization) appear to have evolved multiple times through neofunctionalization in a gene family. This was observed in *Arabidopsis*, poplar, and *Zinnia elegans* (Figure 5; Table S1).

Nonetheless, recent studies have pointed out that sets of amino acid residues, mostly at or close to the enzyme active site, have been positively selected for and thus might be useful in function prediction [14,61,62]. The present study also showed phylogenetic clustering of *PRX* genes from different taxa, and this could be used to predict functional similarity among

the genes. As examples, GhPOD (Malvaceae) and ppa008309m (Rosaceae), which were implicated in male reproduction, belonged to the same clade as AtPRX40 (Brassicaceae) (Figure 5). AtPRX40 functions as an extensin peroxidase during anther development [63], and GhPOD, ppa008309m, and some other genes in the same clade may share the same function. No bryophyte *PRX* gene has been shown to be involved in sporophyte development, although ROS were required in spore wall formation [64]. The three *PpPRX* genes in the AtPRX40 clade (*PpPRX9*, *PpPRX15*, *PpPRX37*) are highly expressed in developing sporophytes (Figure 4), and *PpPRX9*, in particular, was upregulated in the sporophyte transcriptome and coexpressed with sporopollenin biosynthetic genes [65]. Functional characterization of these *PpPRX* genes will reveal the extent of functional similarity in the AtPRX40 clade. Similarly, studies on *PpPRX34* and *PpPRX39* in the ancient land plant-wide clade will be informative regarding ancient functions of embryophyte *PRX* genes and the extent of gene functional similarity in the land plant-wide clade.

5. Conclusions

Forty-nine *PpPRX* genes were identified and their sequences and gene architecture were analyzed. WGDs were mostly responsible for the family expansion, and duplicated genes were under purifying selection, while generally sharing similar expression profiles. A phylogenetic reconstruction with PRX sequences from the major lineages of land plants revealed an ancient land plant-wide clade. Due to the relatively smaller size of the gene family and simpler morphology and physiology of the moss, the *PpPRX* gene family may prove to be a fertile system for functional studies of PRX genes. *PpPRX34* and *PpPRX39* are proposed as candidate genes to test this premise.

Supplementary Materials: The following supporting information can be downloaded at: https://www.mdpi.com/article/10.3390/ijpb15040079/s1, Table S1: Class III peroxidases with reported *in planta* functions; Table S2: Embryophyte class III peroxidases used to reconstruct the Maximum-Likelihood phylogenetic tree: Gene ID and sequence; Figure S1: Amino acid sequence alignment of class III peroxidases from *P. patens*; Figure S2: Expression of *PpPRX7*, *PpPRX9*, and *PpPRX32* in different tissues of *P. patens*. References [8–10,17,22,45,46,63,66–115] are cited in the Supplementary Materials.

Author Contributions: Conceptualization, D.-Y.S.; methodology, validation, formal analysis, investigation, data curation, V.P.M.A., F.R., T.M., W.A.B., E.I.B., and D.-Y.S.; writing—original draft preparation, V.P.M.A., E.I.B., and D.-Y.S.; writing—review and editing, V.P.M.A., E.I.B., and D.-Y.S.; supervision, project administration, funding acquisition, D.-Y.S. All authors have read and agreed to the published version of the manuscript.

Funding: This research was funded by a Natural Sciences and Engineering Research Council of Canada Discovery grant (RGPIN-2018-04286). F.R., T.M., and V.P.M.A. were supported in part by University of Regina Graduate Scholarships. F.R. was a Saskatchewan Innovation Opportunity Graduate Scholarship recipient. W.A.B. was supported by an NSERC Undergraduate Summer Research Award.

Institutional Review Board Statement: Not applicable.

Informed Consent Statement: Not applicable.

Data Availability Statement: The original contributions presented in the study are included in the article/Supplementary Materials. Further inquiries can be directed to the corresponding author.

Conflicts of Interest: The authors declare no conflicts of interest.

References

1. Passardi, F.; Theiler, G.; Zamocky, M.; Cosio, C.; Rouhier, N.; Teixera, F.; Margis-Pinheiro, M.; Ioannidis, V.; Penel, C.; Falquet, L.; et al. PeroxiBase: The peroxidase database. *Phytochemistry* **2007**, *68*, 1605–1611. [CrossRef] [PubMed]
2. Zámocký, M.; Hofbauer, S.; Schaffner, I.; Gasselhuber, B.; Nicolussi, A.; Soudi, M.; Pirker, K.F.; Furtmüller, P.G.; Obingera, C. Independent evolution of four heme peroxidase superfamilies. *Arch. Biochem. Biophys.* **2015**, *574*, 108–119. [CrossRef] [PubMed]
3. Welinder, K.G. Superfamily of plant, fungal and bacterial peroxidases. *Curr. Opin. Struct. Biol.* **1992**, *2*, 388–393. [CrossRef]

4. Mbadinga Mbadinga, D.L.; Li, Q.; Ranocha, P.; Martinez, Y.; Dunand, C. Global analysis of non-animal peroxidases provides insights into the evolution of this gene family in the green lineage. *J. Exp. Bot.* **2020**, *71*, 3350–3360. [CrossRef] [PubMed]
5. Veitch, N.C. Horseradish peroxidase: A modern view of a classic enzyme. *Phytochemistry* **2004**, *65*, 249–259. [CrossRef]
6. Cosio, C.; Dunand, C. Specific functions of individual class III peroxidase genes. *J. Exp. Bot.* **2009**, *60*, 391–408. [CrossRef]
7. Shigeto, J.; Tsutsumi, Y. Diverse functions and reactions of class III peroxidases. *New Phytol.* **2016**, *209*, 1395–1402. [CrossRef]
8. Shigeto, J.; Itoh, Y.; Hirao, S.; Ohira, K.; Fujita, K.; Tsutsumi, Y. Simultaneously disrupting AtPrx2, AtPrx25 and AtPrx71 alters lignin content and structure in *Arabidopsis* stem. *J. Integr. Plant Biol.* **2015**, *57*, 349–356. [CrossRef]
9. Choi, H.W.; Kim, Y.J.; Lee, S.C.; Hong, J.K.; Hwang, B.K. Hydrogen peroxide generation by the pepper extracellular peroxidase $CaPO_2$ activates local and systemic cell death and defense response to bacterial pathogens. *Plant Physiol.* **2007**, *145*, 890–904. [CrossRef]
10. Linkies, A.; Schuster-Sherpa, U.; Tintelnot, S.; Leubner-Metzger, G.; Müller, K. Peroxidases identified in a subtractive cDNA library approach show tissue-specific transcript abundance and enzyme activity during seed germination of *Lepidium sativum*. *J. Exp. Bot.* **2010**, *61*, 491–502. [CrossRef]
11. Tognolli, M.; Penel, C.; Greppin, H.; Simon, P. Analysis and expression of the class III peroxidase large gene family in *Arabidopsis thaliana*. *Gene* **2002**, *288*, 129–138. [CrossRef] [PubMed]
12. Welinder, K.G.; Justesen, A.F.; Kjærsgård, I.V.H.; Jensen, R.B.; Rasmussen, S.K.; Jespersen, H.M.; Duroux, L. Structural diversity and transcription of class III peroxidases from *Arabidopsis thaliana*. *Eur. J. Biochem.* **2002**, *269*, 6063–6081. [CrossRef] [PubMed]
13. Passardi, F.; Longet, D.; Penel, C.; Dunand, C. The class III peroxidase multigenic family in rice and its evolution in land plants. *Phytochemistry* **2004**, *65*, 1879–1893. [CrossRef] [PubMed]
14. Ren, L.L.; Liu, Y.J.; Liu, H.J.; Qian, T.T.; Qi, L.W.; Wang, X.R.; Zeng, Q.Y. Subcellular relocalization and positive selection play key roles in the retention of duplicate genes of Populus class III peroxidase family. *Plant Cell* **2014**, *26*, 2404–2419. [CrossRef] [PubMed]
15. Wang, Y.; Wang, Q.; Zhao, Y.; Han, G.; Zhu, S. Systematic analysis of maize class III peroxidase gene family reveals a conserved subfamily involved in abiotic stress response. *Gene* **2015**, *566*, 95–108. [CrossRef]
16. Cao, Y.; Han, Y.; Meng, D.; Li, D.; Jin, Q.; Lin, Y.; Cai, Y. Structural, evolutionary, and functional analysis of the class III peroxidase gene family in Chinese pear (*Pyrus bretschneideri*). *Front. Plant Sci.* **2016**, *7*, 1874. [CrossRef]
17. Moural, T.W.; Lewis, K.M.; Barnaba, C.; Zhu, F.; Palmer, N.A.; Sarath, G.; Scully, E.D.; Jones, J.P.; Sattler, S.E.; Kang, C. Characterization of class III peroxidases from switchgrass. *Plant Physiol.* **2017**, *173*, 417–433. [CrossRef]
18. Yan, J.; Su, P.; Li, W.; Xiao, G.; Zhao, Y.; Ma, X.; Wang, H.; Nevo, E.; Kong, L. Genome-wide and evolutionary analysis of the class III peroxidase gene family in wheat and *Aegilops tauschii* reveals that some members are involved in stress responses. *BMC Genom.* **2019**, *20*, 666. [CrossRef]
19. Chen, Y.; Feng, J.; Qu, Y.; Zhang, J.; Zhang, L.; Liang, D.; Yang, Y.; Huang, J. Genome-wide identification and functional analysis of class III peroxidases in *Gossypium hirsutum*. *PeerJ* **2022**, *10*, e13635. [CrossRef]
20. Xiao, H.; Wang, C.; Khan, N.; Chen, M.; Fu, W.; Guan, L. Genome-wide identification of the class III *POD* gene family and their expression profiling in grapevine (*Vitis vinifera* L). *BMC Genom.* **2020**, *21*, 444. [CrossRef]
21. Yang, X.; Yuan, J.; Luo, W.; Qin, M.; Yang, J.; Wu, W.; Xie, X. Genome-wide identification and expression analysis of the class III peroxidase gene family in potato (*Solanum tuberosum* L.). *Front. Genet.* **2020**, *11*, 593577. [CrossRef] [PubMed]
22. Aleem, M.; Riaz, A.; Raza, Q.; Aleem, M.; Aslam, M.; Kong, K.; Atif, R.M.; Kashif, M.; Bhat, J.A.; Zhao, T. Genome-wide characterization and functional analysis of class III peroxidase gene family in soybean reveal regulatory roles of GsPOD40 in drought tolerance. *Genomics* **2022**, *114*, 45–60. [CrossRef] [PubMed]
23. Cheng, L.; Ma, L.; Meng, L.; Shang, H.; Cao, P.; Jin, J. Genome-wide identification and analysis of the class III peroxidase gene family in tobacco (*Nicotiana tabacum*). *Front. Genet.* **2022**, *13*, 916867. [CrossRef] [PubMed]
24. Duroux, L.; Welinder, K.G. The peroxidase gene family in plants: A phylogenetic overview. *J. Mol. Evol.* **2003**, *57*, 397–407. [CrossRef]
25. Oliveira, R.A.d.C.; de Andrade, A.S.; Imparato, D.O.; de Lima, J.G.S.; de Almeida, R.V.M.; Lima, J.P.M.S.; Pasquali, M.A.B.; Dalmolin, R.J.S. Analysis of *Arabidopsis thaliana* redox gene network indicates evolutionary expansion of class III peroxidase in plants. *Sci. Rep.* **2019**, *9*, 15741. [CrossRef]
26. Francoz, E.; Ranocha, P.; Nguyen-Kim, H.; Jamet, E.; Burlat, V.; Dunand, C. Roles of cell wall peroxidases in plant development. *Phytochemistry* **2015**, *112*, 15–21. [CrossRef]
27. Rensing, S.A.; Goffinet, B.; Meyberg, R.; Wu, S.-Z.; Bezanilla, M. The moss *Physcomitrium* (*Physcomitrella*) *patens*: A model organism for non-seed plants. *Plant Cell* **2020**, *32*, 1361–1376. [CrossRef]
28. Hohe, A.; Egener, T.; Lucht, J.M.; Holtorf, H.; Reinhard, C.; Schween, G.; Reski, R. An improved and highly standardized transformation procedure allows efficient production of single and multiple targeted gene knockouts in a moss, *Physcomitrella patens*. *Current Genet.* **2004**, *44*, 339–347.
29. Fernandez-Pozo, N.; Haas, F.B.; Meyberg, R.; Ullrich, K.K.; Hiss, M.; Perroud, P.-F.; Hanke, S.; Kratz, V.; Powell, A.F.; Vesty, E.F.; et al. PEATmoss (Physcomitrella Expression Atlas Tool): A unified gene expression atlas for the model plant *Physcomitrella patens*. *Plant J.* **2020**, *102*, 165–177. [CrossRef]
30. Strotbek, C.; Krinninger, S.; Frank, W. The moss *Physcomitrella patens*: Methods and tools from cultivation to targeted analysis of gene function. *Int. J. Dev. Biol.* **2013**, *57*, 553–564. [CrossRef]

31. Lehtonen, M.T.; Akita, M.; Kalkkinen, N.; Ahola-Iivarinen, E.; Rönnholm, G.; Somervuo, P.; Thelander, M.; Valkonen, J.P.T. Quickly-released peroxidase of moss in defense against fungal invaders. *New Phytol.* **2009**, *183*, 432–443. [CrossRef] [PubMed]
32. Savelli, B.; Li, Q.; Webber, M.; Jemmat, A.M.; Robitaille, A.; Zamocky, M.; Mathé, C.; Dunand, C. RedoxiBase: A database for ROS homeostasis regulated proteins. *Redox Biol.* **2019**, *26*, 101247. [CrossRef] [PubMed]
33. Thumuluri, V.; Almagro Armenteros, J.J.; Johansen, A.R.; Nielsen, H.; Winther, O. DeepLoc 2.0: Multi-label subcellular localization prediction using protein language models. *Nucleic Acids Res.* **2022**, *50*, W228–W234. [CrossRef] [PubMed]
34. Käll, L.; Krogh, A.; Sonnhammer, E.L.L. A combined transmembrane topology and signal peptide prediction method. *J. Mol. Biol.* **2004**, *338*, 1027–1036. [CrossRef] [PubMed]
35. Kumar, S.; Stecher, G.; Li, M.; Knyaz, C.; Tamura, K. MEGA X: Molecular evolutionary genetics analysis across computing platforms. *Mol. Biol. Evol.* **2018**, *35*, 1547–1549. [CrossRef]
36. Letunic, I.; Bork, P. Interactive Tree Of Life (iTOL) v4: Recent updates and new developments. *Nucleic Acids Res.* **2019**, *47*, W256–W259. [CrossRef]
37. Miller, M.A.; Pfeiffer, W.; Schwartz, T. Creating the CIPRES Science Gateway for inference of large phylogenetic trees. In Proceedings of the Gateway Computing Environments Workshop (GCE), New Orleans, LA, USA, 14 November 2010; pp. 1–8. [CrossRef]
38. Lang, D.; Ullrich, K.K.; Murat, F.; Fuchs, J.; Jenkins, J.; Haas, F.B.; Piednoel, M.; Gundlach, H.; Van Bel, M.; Meyberg, R.; et al. The *Physcomitrella patens* chromosome-scale assembly reveals moss genome structure and evolution. *Plant J.* **2018**, *93*, 515–533. [CrossRef]
39. Wernersson, R.; Pedersen, A.G. RevTrans: Multiple alignment of coding DNA from aligned amino acid sequences. *Nucleic Acids Res.* **2003**, *31*, 3537–3539. [CrossRef]
40. Rozas, J.; Ferrer-Mata, A.; Sánchez-DelBarrio, J.C.; Guirao-Rico, S.; Librado, P.; Ramos-Onsins, S.E.; Sánchez-Gracia, A. DnaSP 6: DNA sequence polymorphism analysis of large data sets. *Mol. Biol. Evol.* **2017**, *34*, 3299–3302. [CrossRef]
41. Ortiz-Ramírez, C.; Hernandez-Coronado, M.; Thamm, A.; Catarino, B.; Wang, M.; Dolan, L.; Feijó, J.A.; Becker, J.D. A transcriptome atlas of *Physcomitrella patens* provides insights into the evolution and development of land plants. *Mol. Plant* **2016**, *9*, 205–220. [CrossRef]
42. Mathé, C.; Dunand, C. Automatic prediction and annotation: There are strong biases for multigenic families. *Front. Genet.* **2021**, *12*, 697477. [CrossRef] [PubMed]
43. Lüthje, S.; Martinez-Cortes, T. Membrane-Bound Class III Peroxidases: Unexpected enzymes with exciting functions. *Int. J. Mol. Sci.* **2018**, *19*, 2876. [CrossRef] [PubMed]
44. Lehtonen, M.T.; Takikawa, Y.; Rönnholm, G.; Akita, M.; Kalkkinen, N.; Ahola-Iivarinen, E.; Somervuo, P.; Varjosalo, M.; Valkonen, J.P. Protein secretome of moss plants (*Physcomitrella patens*) with emphasis on changes induced by a fungal elicitor. *J. Proteome Res.* **2014**, *13*, 447–459. [CrossRef] [PubMed]
45. Lehtonen, M.T.; Akita, M.; Frank, W.; Reski, R.; Valkonen, J.P.T. Involvement of a class III peroxidase and the mitochondrial protein TSPO in oxidative burst upon treatment of moss plants with a fungal elicitor. *Mol. Plant Microbe Interact.* **2012**, *25*, 363–371. [CrossRef] [PubMed]
46. Martínez-Cortés, T.; Pomar, F.; Merino, F.; Novo-Uzal, E. A proteomic approach to *Physcomitrella patens* rhizoid exudates. *J. Plant Physiol.* **2014**, *171*, 1671–1678. [CrossRef]
47. Martínez-Cortés, T.; Pomar, F.; Novo-Uzal, E. Evolutionary implications of a peroxidase with high affinity for cinnamyl alcohols from *Physcomitrium patens*, a non-vascular plant. *Plants* **2021**, *10*, 1476. [CrossRef]
48. Mathé, C.; Barre, A.; Jourda, C.; Dunand, C. Evolution and expression of class III peroxidases. *Arch. Biochem. Biophys.* **2010**, *500*, 58–65. [CrossRef]
49. Roy, S.W.; Penny, D. Patterns of intron loss and gain in plants: Intron loss–dominated evolution and genome-wide comparison of *O. sativa* and *A. thaliana*. *Mol. Biol. Evol.* **2007**, *24*, 171–181. [CrossRef]
50. Simões, M.S.; Carvalho, G.G.; Ferreira, S.S.; Cesarino, I. Toward the identification of class III peroxidases potentially involved in lignification in the model C4 grass *Setaria viridis*. *Theor. Exp. Plant Physiol.* **2023**, *35*, 111–131. [CrossRef]
51. Casneuf, T.; De Bodt, S.; Raes, J.; Maere, S.; Van de Peer, Y. Nonrandom divergence of gene expression following gene and genome duplications in the flowering plant *Arabidopsis thaliana*. *Genome Biol.* **2006**, *7*, R13. [CrossRef]
52. Rodgers-Melnick, E.; Mane, S.P.; Dharmawardhana, P.; Slavov, G.T.; Crasta, O.R.; Strauss, S.H.; Brunner, A.M.; Difazio, S.P. Contrasting patterns of evolution following whole genome versus tandem duplication events in *Populus*. *Genome Res.* **2012**, *22*, 95–105. [CrossRef] [PubMed]
53. Qiao, X.; Yin, H.; Li, L.; Wang, R.; Wu, J.; Wu, J.; Zhang, S. Different modes of gene duplication show divergent evolutionary patterns and contribute differently to the expansion of gene families involved in important fruit traits in pear (*Pyrus bretschneideri*). *Front. Plant Sci.* **2018**, *9*, 161. [CrossRef] [PubMed]
54. Zhu, T.; Xin, F.; Wei, S.; Liu, Y.; Han, Y.; Xie, J.; Ding, Q.; Ma, L. Genome-wide identification, phylogeny and expression profiling of class III peroxidases gene family in *Brachypodium distachyon*. *Gene* **2019**, *700*, 149–162. [CrossRef] [PubMed]
55. Meng, G.; Fan, W.; Rasmussen, S.K. Characterisation of the class III peroxidase gene family in carrot taproots and its role in anthocyanin and lignin accumulation. *Plant Physiol. Biochem.* **2021**, *167*, 245–256. [CrossRef] [PubMed]
56. Cai, K.; Liu, H.; Chen, S.; Liu, Y.; Zhao, X.; Chen, S. Genome-wide identification and analysis of class III peroxidases in *Betula pendula*. *BMC Genom.* **2021**, *22*, 314. [CrossRef] [PubMed]

57. Kjærsgård, I.V.H.; Jespersen, H.M.; Rasmussen, S.K.; Welinder, K.G. Sequence and RT-PCR expression analysis of two peroxidases from *Arabidopsis thaliana* belonging to a novel evolutionary branch of plant peroxidases. *Plant Mol. Biol.* **1997**, *33*, 699–708. [CrossRef]
58. Valério, L.; Meyer, M.D.; Penel, C.; Dunand, C. Expression analysis of the *Arabidopsis* peroxidase multigenic family. *Phytochemistry* **2004**, *65*, 1331–1342. [CrossRef]
59. Hoffmann, N.; Benske, A.; Betz, H.; Schuetz, M.; Samuels, A.L. Laccases and peroxidases co-localize in lignified secondary cell walls throughout stem development. *Plant Physiol.* **2020**, *184*, 806–822. [CrossRef]
60. Passardi, F.; Cosio, C.; Penel, C.; Dunand, C. Peroxidases have more functions than a Swiss army knife. *Plant Cell Rep.* **2005**, *24*, 255–265. [CrossRef]
61. Kupriyanova, E.V.; Mamoshina, P.O.; Ezhova, T.A. Evolutionary divergence of *Arabidopsis thaliana* classical peroxidases. *Biochemistry* **2015**, *80*, 1362–1372. [CrossRef]
62. New, J.; Barsky, D.; Uhde-Stone, C. ROS consumers or producers? Interpreting transcriptomic data by AlphaFold modeling provides insights into class III peroxidase functions in response to biotic and abiotic stresses. *Int. J. Mol. Sci.* **2023**, *24*, 8297. [CrossRef]
63. Jacobowitz, J.R.; Doyle, W.C.; Weng, J.-K. PRX9 and PRX40 are extensin peroxidases essential for maintaining tapetum and microspore cell wall integrity during *Arabidopsis* anther development. *Plant Cell* **2019**, *31*, 848–861. [CrossRef] [PubMed]
64. Rabbi, F.; Renzaglia, K.S.; Ashton, N.W.; Suh, D.-Y. Reactive oxygen species are required for spore-wall formation in *Physcomitrella patens*. *Botany* **2020**, *98*, 575–587. [CrossRef] [PubMed]
65. O'Donoghue, T.-M.; Chater, C.; Wallace, S.; Gray, J.E.; Beerling, D.J.; Fleming, A.J. Genome-wide transcriptomic analysis of the sporophyte of the moss *Physcomitrella patens*. *J. Exp. Bot.* **2013**, *64*, 3567–3581. [CrossRef] [PubMed]
66. Aoyama, W.; Sasaki, S.; Matsumura, S.; Mitsunaga, T.; Hirai, H.; Tsutsumi, Y.; Nishida, T. Sinapyl alcohol-specific peroxidase isoenzyme catalyzes the formation of the dehydrogenative polymer from sinapyl alcohol. *J. Wood Sci.* **2002**, *48*, 497–504. [CrossRef]
67. Blee, K.A.; Choi, J.W.; O'Connell, A.P.; Schuch, W.; Lewis, N.G.; Bolwell, G. A lignin-specific peroxidase in tobacco whose antisense suppression leads to vascular tissue modification. *Phytochemistry* **2003**, *64*, 163–176. [CrossRef]
68. Chang, C.-L.; Serapion, J.C.; Hung, H.-H.; Lin, Y.-C.; Tsai, Y.-C.; Jane, W.-N.; Chang, M.-C.; Lai, M.-H.; Hsing, Y.-I.C. Studies of a rice sterile mutant *sstl* from the TRIM collection. *Bot. Stud.* **2019**, *60*, 12. [CrossRef]
69. Chen, D.; Ding, Y.; Guo, W.; Zhang, T. Molecular cloning and characterization of a flower-specific class III peroxidase gene in G. Hirsutum. *Mol. Biol. Rep.* **2009**, *36*, 461–469. [CrossRef]
70. Christensen, J.H.; Bauw, G.; Welinder, K.G.; Van Montagu, M.; Boerjan, W. Purification and Characterization of Peroxidases Correlated with Lignification in Poplar Xylem. *Plant Physiol.* **1998**, *118*, 125–135. [CrossRef]
71. Cosio, C.; Ranocha, P.; Francoz, E.; Burlat, V.; Zheng, Y.; Perry, S.E.; Ripoll, J.; Yanofsky, M.; Dunand, C. The class III peroxidase PRX17 is a direct target of the MADS-box transcription factor AGAMOUS-LIKE15 (AGL15) and participates in lignified tissue formation. *New Phytol.* **2017**, *213*, 250–263. [CrossRef]
72. Cosio, C.; Vuillemin, L.; De Meyer, M.; Kevers, C.; Penel, C.; Dunand, C. An anionic class III peroxidase from zucchini may regulate hypocotyl elongation thanks to its auxin oxidase activity. *Planta* **2009**, *229*, 823–836. [CrossRef] [PubMed]
73. Costa, M.M.R.; Hilliou, F.; Duarte, P.; Pereira, L.G.; Almeida, I.; Leech, M.; Memelink, J.; Barceló, A.R.; Sottomayor, M. Molecular Cloning and Characterization of a Vacuolar Class III Peroxidase Involved in the Metabolism of Anticancer Alkaloids in *Catharanthus roseus*. *Plant Physiol.* **2008**, *146*, 403–417. [CrossRef] [PubMed]
74. El Mansouri, I.; Mercado, J.A.; Valpuesta, V.; Quesada, M.A.; Santiago-Dómenech, N.; Pliego-Alfaro, F. Biochemical and phenotypical characterization of transgenic tomato plants overexpressing a basic peroxidase. *Physiol. Plant.* **1999**, *106*, 355–362. [CrossRef]
75. Fernández-Pérez, F.; Pomar, F.; Pedreño, M.A.; Novo-Uzal, E. The suppression of *AtPrx52* affects fibers but not xylem lignification in *Arabidopsis* by altering the proportion of syringyl units. *Physiol. Plant.* **2015**, *154*, 395–406. [CrossRef] [PubMed]
76. Fernández-Pérez, F.; Vivar, T.; Pomar, F.; Pedreño, M.A.; Novo-Uzal, E. Peroxidase 4 is involved in syringyl lignin formation in *Arabidopsis thaliana*. *J. Plant Physiol.* **2015**, *175*, 86–94. [CrossRef]
77. Gabaldón, C.; López-Serrano, M.; Pomar, F.; Merino, F.; Cuello, J.; Pedreño, M.; Barceló, A.R. Characterization of the last step of lignin biosynthesis in *Zinnia elegans* suspension cell cultures. *FEBS Lett.* **2005**, *580*, 4311–4316. [CrossRef]
78. García-Ulloa, A.; Sanjurjo, L.; Cimini, S.; Encina, A.; Martínez-Rubio, R.; Bouza, R.; Barral, L.; Estévez-Pérez, G.; Novo-Uzal, E.; De Gara, L.; et al. Overexpression of ZePrx in *Nicotiana tabacum* affects lignin biosynthesis without altering redox homeostasis. *Front. Plant Sci.* **2020**, *11*, 900. [CrossRef]
79. Herrero, J.; Fernández-Pérez, F.; Yebra, T.; Novo-Uzal, E.; Pomar, F.; Pedreño, M.; Cuello, J.; Guéra, A.; Esteban-Carrasco, A.; Zapata, J.M. Bioinformatic and functional characterization of the basic peroxidase 72 from *Arabidopsis thaliana* involved in lignin biosynthesis. *Planta* **2013**, *237*, 1599–1612. [CrossRef]
80. Jemmat, A.M.; Ranocha, P.; Le Ru, A.; Neel, M.; Jauneau, A.; Raggi, S.; Ferrari, S.; Burlat, V.; Dunand, C. Coordination of five class III peroxidase-encoding genes for early germination events of *Arabidopsis thaliana*. *Plant Sci.* **2020**, *298*, 110565. [CrossRef]
81. Jeong, Y.J.; Kim, Y.-C.; Lee, J.S.; Kim, D.-G.; Lee, J.H. Reduced expression of PRX2/ATPRX1, PRX8, PRX35, and PRX73 affects cell elongation, vegetative growth, and vasculature structures in *Arabidopsis thaliana*. *Plants* **2022**, *11*, 3353. [CrossRef]

82. Kámán-Tóth, E.; Dankó, T.; Gullner, G.; Bozsó Palkovics, L.; Pogány, M. Contribution of cell wall peroxidase and NADPH oxidase-derived reactive oxygen species to Alternaria brassicicola-induced oxidative burst in *Arabidopsis*. *Mol. Plant Pathol.* **2019**, *20*, 485–499. [CrossRef] [PubMed]
83. Kidwai, M.; Dhar, Y.V.; Gautam, N.; Tiwari, M.; Ahmad, I.Z.; Asif, M.H.; Chakrabarty, D. Oryza sativa class III peroxidase (OsPRX38) overexpression in *Arabidopsis thaliana* reduces arsenic accumulation due to apoplastic lignification. *J. Hazard. Mater.* **2019**, *362*, 383–393. [CrossRef] [PubMed]
84. Kim, M.J.; Ciani, S.; Schachtman, D.P. A Peroxidase Contributes to ROS Production during *Arabidopsis* Root Response to Potassium Deficiency. *Mol. Plant* **2010**, *3*, 420–427. [CrossRef] [PubMed]
85. Kim, Y.-H.; Kim, H.S.; Park, S.-C.; Ji, C.Y.; Yang, J.; Lee, H.; Kwak, S.-S. Overexpression of *swpa4* peroxidase enhances tolerance to hydrogen peroxide and high salinity-mediated oxidative stress in transgenic sweetpotato plants. *Plant Biotechnol. Rep.* **2020**, *14*, 301–307. [CrossRef]
86. Kim, Y.-H.; Kim, H.S.; Park, S.-C.; Ji, C.Y.; Yang, J.-W.; Lee, H.-U.; Kwak, S.-S. Downregulation of swpa4 peroxidase expression in transgenic sweetpotato plants decreases abiotic stress tolerance and reduces stress-related peroxidase expression. *Plant Biotechnol. Rep.* **2021**, *15*, 69–76. [CrossRef]
87. Kunieda, T.; Shimada, T.; Kondo, M.; Nishimura, M.; Nishitani, K.; Hara-Nishimura, I. Spatiotemporal Secretion of PEROXIDASE36 Is Required for Seed Coat Mucilage Extrusion in *Arabidopsis*. *Plant Cell* **2013**, *25*, 1355–1367. [CrossRef]
88. Laitinen, T.; Morreel, K.; Delhomme, N.; Gauthier, A.; Schiffthaler, B.; Nickolov, K.; Brader, G.; Lim, K.J.; Teeri, T.H.; Street, N.R.; et al. A key role for apoplastic H_2O_2 in Norway spruce phenolic metabolism. *Plant Physiol.* **2017**, *174*, 1449–1475. [CrossRef]
89. Lee, Y.; Rubio, M.C.; Alassimone, J.; Geldner, N. A Mechanism for Localized Lignin Deposition in the Endodermis. *Cell* **2013**, *153*, 402–412. [CrossRef]
90. Li, Q.; Qin, X.; Qi, J.; Dou, W.; Dunand, C.; Chen, S.; He, Y. CsPrx25, a class III peroxidase in *Citrus sinensis*, confers resistance to citrus bacterial canker through the maintenance of ROS homeostasis and cell wall lignification. *Hortic. Res.* **2020**, *7*, 192. [CrossRef]
91. Lin, C.-Y.; Li, Q.; Tunlaya-Anukit, S.; Shi, R.; Sun, Y.-H.; Wang, J.P.; Liu, J.; Loziuk, P.; Edmunds, C.W.; Miller, Z.D.; et al. A cell wall-bound anionic peroxidase, PtrPO21, is involved in lignin polymerization in *Populus trichocarpa*. *Tree Genet. Genomes* **2016**, *12*, 22. [CrossRef]
92. Liu, H.; Dong, S.; Li, M.; Gu, F.; Yang, G.; Guo, T.; Chen, Z.; Wang, J. The Class III peroxidase gene *OsPrx30*, transcriptionally modulated by the AT-hook protein OsATH1, mediates rice bacterial blight-induced ROS accumulation. *J. Integr. Plant Biol.* **2021**, *63*, 393–408. [CrossRef] [PubMed]
93. Lorrai, R.; Francocci, F.; Gully, K.; Martens, H.J.; De Lorenzo, G.; Nawrath, C.; Ferrari, S. Impaired cuticle functionality and robust resistance to Botrytis cinerea in *Arabdopsis thaliana* plants with altered homogalacturonan integrity are dependent on the class III peroxidase AtPRX71. *Front. Plant Sci.* **2021**, *12*, 696955. [CrossRef] [PubMed]
94. Martin, R.E.; Marzol, E.; Estevez, J.M.; Muday, G.K. Ethylene signaling increases reactive oxygen species accumulation to drive root hair initiation in *Arabidopsis*. *Development* **2022**, *149*, dev200487. [CrossRef]
95. Marzol, E.; Borassi, C.; Carignani Sardoy, M.; Ranocha, P.; Aptekmann, A.A.; Bringas, M.; Pennington, J.; Paez-Valencia, J.; Martinez Pacheco, J.; Rodríguez-Garcia, D.R.; et al. Class III peroxidases PRX01, PRX44, and PRX73 control root hair growth in *Arabidopsis thaliana*. *Int. J. Mol. Sci.* **2022**, *23*, 5375. [CrossRef] [PubMed]
96. McInnis, S.M.; Costa, L.M.; Gutiérrez-Marcos, J.F.; Henderson, C.A.; Hiscock, S.J. Isolation and characterization of a polymorphic stigma-specific class III peroxidase gene from *Senecio squalidus* L. (Asteraceae). *Plant Mol. Biol.* **2005**, *57*, 659–677. [CrossRef] [PubMed]
97. Mei, W.; Qin, Y.; Song, W.; Li, J.; Zhu, Y. Cotton GhPOX1 encoding plant class III peroxidase may be responsible for the high level of reactive oxygen species production that is related to cotton fiber elongation. *J. Genet. Genom.* **2009**, *36*, 141–150. [CrossRef] [PubMed]
98. Osakabe, K.; Koyama, H.; Kawai, S.; Katayama, Y.; Morohoshi, N. Molecular cloning of two tandemly arranged peroxidase genes from *Populus kitakamiensis* and their differential regulation in the stem. *Plant Mol. Biol.* **1995**, *28*, 677–689. [CrossRef]
99. Østergaard, L.; Teilum, K.; Mirza, O.; Mattsson, O.; Petersen, M.; Welinder, K.G.; Mundy, J.; Gajhede, M.; Henriksen, A. *Arabidopsis* ATP A2 peroxidase. Expression and high-resolution structure of a plant peroxidase with implications for lignification. *Plant Mol. Biol.* **2000**, *44*, 231–243. [CrossRef]
100. Pacheco, J.M.; Ranocha, P.; Kasulin, L.; Fusari, C.M.; Servi, L.; Aptekmann, A.A.; Gabarain, V.B.; Peralta, J.M.; Borassi, C.; Marzol, E.; et al. Apoplastic class III peroxidases PRX62 and PRX69 promote *Arabidopsis* root hair growth at low temperature. *Nat. Commun.* **2022**, *13*, 1310. [CrossRef]
101. Park, S.C.; Pyun, J.W.; Jeong, Y.J.; Park, S.H.; Kim, S.; Kim, Y.H.; Lee, J.R.; Kim, C.Y.; Jeong, J.C. Overexpression of VlPRX21 and VlPRX35 genes in *Arabidopsis* plants leads to bioconversion of trans-resveratrol to δ-viniferin. *Plant Physiol. Biochem.* **2021**, *162*, 556–563. [CrossRef] [PubMed]
102. Passardi, F.; Tognolli, M.; De Meyer, M.; Penel, C.; Dunand, C. Two cell wall associated peroxidases from *Arabidopsis* influence root elongation. *Planta* **2006**, *223*, 965–974. [CrossRef] [PubMed]
103. Ríos, G.; Tadeo, F.R.; Leida, C.; Badenes, M.L. Prediction of components of the sporopollenin synthesis pathway in peach by genomic and expression analyses. *BMC Genom.* **2013**, *14*, 40. [CrossRef] [PubMed]

104. Sasaki, S.; Baba, K.; Nishida, T.; Tsutsumi, Y.; Kondo, R. The cationic cell-wall-peroxidase having oxidation ability for polymeric substrate participates in the late stage of lignification of *Populus alba* L. *Plant Mol. Biol.* **2006**, *62*, 797–807. [CrossRef]
105. Shigeto, J.; Kiyonaga, Y.; Fujita, K.; Kondo, R.; Tsutsumi, Y. Putative Cationic Cell-Wall-Bound Peroxidase Homologues in *Arabidopsis*, AtPrx2, AtPrx25, and AtPrx71, Are Involved in Lignification. *J. Agric. Food Chem.* **2013**, *61*, 3781–3788. [CrossRef]
106. Shigeto, J.; Nagano, M.; Fujita, K.; Tsutsumi, Y. Catalytic Profile of *Arabidopsis* Peroxidases, AtPrx-2, 25 and 71, Contributing to Stem Lignification. *PLoS ONE* **2014**, *9*, e105332. [CrossRef]
107. Su, P.; Yan, J.; Li, W.; Wang, L.; Zhao, J.; Ma, X.; Li, A.; Wang, H.; Kong, L. A member of wheat class III peroxidase gene family, TaPRX-2A, enhanced the tolerance of salt stress. *BMC Plant Biol.* **2020**, *20*, 392. [CrossRef]
108. Swanson, R.; Clark, T.; Preuss, D. Expression profiling of *Arabidopsis* stigma tissue identifies stigma-specific genes. *Sex. Plant Reprod.* **2005**, *18*, 163–171. [CrossRef]
109. Tung, C.-W.; Dwyer, K.G.; Nasrallah, M.E.; Nasrallah, J.B. Genome-Wide Identification of Genes Expressed in *Arabidopsis* Pistils Specifically along the Path of Pollen Tube Growth. *Plant Physiol.* **2005**, *138*, 977–989. [CrossRef]
110. Vatulescu, A.D.; Fortunato, A.S.; Sá, M.C.; Amâncio, S.; Ricardo, C.P.; Jackson, P.A. Cloning and characterisation of a basic IAA oxidase associated with root induction in *Vitis vinifera*. *Plant Physiol. Biochem.* **2004**, *42*, 609–615. [CrossRef]
111. Wang, C.-J.; Chan, Y.-L.; Shien, C.H.; Yeh, K.-W. Molecular characterization of fruit-specific class III peroxidase genes in tomato (*Solanum lycopersicum*). *J. Plant Physiol.* **2015**, *177*, 83–92. [CrossRef] [PubMed]
112. Xie, J.; Qi, B.; Mou, C.; Wang, L.; Jiao, Y.; Dou, Y.; Zheng, H. *BREVIPEDICELLUS* and *ERECTA* control the expression of *AtPRX17* to prevent *Arabidopsis callus* browning. *J. Exp. Bot.* **2022**, *73*, 1516–1532. [CrossRef] [PubMed]
113. Yang, X.-J.; Fu, Y.-Q.; Ma, S.; Gan, H.; Xu, W.; Shen, H. The class III peroxidase gene *OsPrx24* is important for root Iron plaque formation and benefits phosphorus uptake in Rice plants under alternate wetting and drying irrigation. *Plant Soil* **2020**, *448*, 621–646. [CrossRef]
114. Zhao, L.; Phuong, L.T.; Luan, M.T.; Fitrianti, A.N.; Matsui, H.; Nakagami, H.; Noutoshi, Y.; Yamamoto, M.; Ichinose, Y.; Shiraishi, T.; et al. A class III peroxidase PRX34 is a component of disease resistance in *Arabidopsis*. *J. Gen. Plant Pathol.* **2019**, *85*, 405–412. [CrossRef]
115. Zimmerlin, A.; Wojtaszek, P.; Bolwell, G.P. Synthesis of dehydrogenation polymers of ferulic acid with high specificity by a purified cell-wall peroxidase from French bean (*Phaseolus vulgaris* L.). *Biochem. J.* **1994**, *299*, 747–753. [CrossRef]